16th ICAAR LISBOA 2020-2022

16th International Conference on
Alkali-Aggregate Reaction in Concrete
Lisboa | LNEC | Portugal | 31 May - 2 June 2022

http://icaar2020-2022.lnec.pt

Microstructural Study of the Chemical and Physical Nature of Alkali Silica Reaction with Emphasis on Reaction Sites

Per Hagelia [(1)], Isabel Fernandes [(2)]

(1) Norwegian Public Roads Administration, Oslo, Norway (per.hagelia@vegvesen.no)

(2) University of Lisbon/IDL, Lisbon, Portugal (mifernandes@fc.ul.pt)

Abstract

The present study focused on ASR-gels in microcracks within reacted aggregates and cement pastes and in air voids, their microstructural setting and detailed chemical analyses of gels using electron microprobe. Chemical variations show that ASR-gels are two-component mixtures of a negatively charged Si-Ca amorphous network and a liquid, where K and Na likely contributed to swelling by electrical double layer repulsion. The composition of single gels varied very much, reflecting the local aggregate mineralogy and proximity to the cement paste. Calculated compressive strengths and swelling pressures were mainly between 10-20 MPa and 0.2-1 MPa, respectively. Textures, compositions, high gel strengths (reflecting high viscosities) and swelling pressures suggest that crack-bound gels accumulated and acted in situ and did not move from aggregates into the cement paste. The development of ASR involved early-stage attack of fluids from the cement paste along foliation planes and pre-existing microcracks. This was followed by gel accumulation within aggregate cracks causing expansion. Crack propagation into the cement paste with in situ formation of layered ASR-gel in the paste apparently depended on gel strength and gel accumulation in the aggregates: Relatively weak gels in aggregates did not cause crack propagation into the paste. Our data suggest that sequential accumulation of ASR-gels, having molar volumes similar to gypsum, might be more important than the effect of gel swelling pressures in the development of deleterious expansion.

***Keywords**: expansion mechanism; gel composition; gel distribution; microstructure; rheology*

1. ALKALI SILICA REACTION AND SIGNIFICANCE OF REACTION SITE CHARACTERISATION

Alkali Silica Reactions (ASR) in concrete involve chemical reactions between the pore solution and reactive aggregates, leading to formation of expanding viscoelastic Na_2O-K_2O-CaO-SiO_2-H_2O gels with high yield strength. ASR may ultimately lead to deleterious micro- and macrocracking of concrete, usually after some decades. A prerequisite for such behaviour is that the formation conditions for such gels can be sustained for a long period of time (cf. [1,2,3]).

The expansive gels form by chemical reaction between silicon derived from reactive silica in the concrete aggregates and dissolved Na, K, Ca and hydroxyl ions in highly alkaline cement paste. The level of ASR increases with the alkali content of the cement used. However, alkalis and silicon can also be released from silicates such as feldspars and micas in the aggregate at high pH, which further sustains formation of ASR gels [4,5,6]. Hence, where feldspars and micas are present, ASR is not solely influenced by the alkali contents of the cements. Taken together the general term alkali silicate reaction would perhaps seem more appropriate, encompassing pure alkali silica reaction with Si released from silica such as opal, chalcedony, crypto or microcrystalline silica and with variable contributions of Na, K and Si released by dissolution of micas and feldspars in rocks such as gneiss or mylonite.

The occurrence of expansive ASR-gels and/or crystalline reaction products and associated development of cracks is typically inhomogeneously distributed at different scales, reflecting the intrinsically inhomogeneous nature of ASR. Single reactive aggregate particles commonly show localised sites where most gels occur, whilst large portions of the same reactive particle have for some reason been left without obvious traces of reaction. Similarly, the accumulation of gels within the cement paste matrix in cracks and voids is inhomogeneously. Furthermore, there are many documented examples in the literature where gels do not fill the interior parts of aggregate cracks. This is characterised by an empty space towards which the gels terminate, whilst gels extending into the cement paste outside usually fill the crack space completely [7,8,9]. Some workers consider that gels

initially formed within the aggregate particles can move outwards into the cement paste [10,11]. However, this mechanism might not be regarded as a rule and should generally be scrutinised in view of petrographic and chemical evidence. The highly variable petrographic features of both pristine concrete and subsequent ASR-affected concrete suggest that a homogeneous distribution of chemical components and conditions for alkali-silica reaction cannot be assumed. Implicitly this suggest that highly reactive and less reactive micro-domains and gels with contrasting swelling properties may exist side by side.

In order to better understand the development of ASR in concrete it is important to investigate the full petrographic variation. The detailed microstructural and chemical characterisation of gels, their contact relations with aggregate minerals, microcracks and voids represents a very important basis for further insight into ASR [8,12]. However, unfortunately this approach has not yet been fully utilised. The compositional variation within single gels in various settings remains to be investigated.

1.1 Conditions for gel formation and swelling in view of petrography and micro-chemistry

Micro-cracking and surface map-cracking requires that gel swelling pressures exceed the tensile strength of concrete at some point in time. The tensile strengths of cement pastes and quartz and feldspar-rich aggregates are commonly found to be approximately 2-2,5 MPa and 8-18 MPa, respectively [13,14,15]. Gel swelling pressures vary from less than 1 MPa in sodium-rich gels to about 11 MPa, and probably rarely exceed 6-7 MPa [16,17]. Calculations based on electrical double-layer theory have yielded gel swelling pressures of about 5-11 MPa [18], whilst compressive strengths of experimental gels vary from 0.5 MPa to 11.3 MPa [3]. In view of this, it may be assumed that ASR gel swelling pressures more likely exceed the tensile strength of cement pastes than the tensile strength of high-quality aggregate particles. However, hydration of silicates [19] and amorphisation during dissolution of silica [20], causes chemical softening of initially strong aggregates. Hence, ASR is a chemical strain softening reaction which should reduce the tensile strength of reacting aggregates [2] and the direct tensile strength of concrete in up to 80% [21]. Intuitively, pre-existing permeable microcracks might represent the weakest sites in this respect, as was also demonstrated by [11].

ASR involves dissolution of silica at high pH in presence of alkalis and calcium, with subsequent polymerisation and formation of swelling ASR-gels. Dissolution of pure silica takes place as follows [22]: The hydroxyl ions in the concrete pore fluid attack the siloxane bridges (Si-O-Si), forming unstable sites predominated by silanol groups (Si-OH-). Subsequent adsorption of oriented molecular water on the silanol groups leads to dissociation and formation of negatively charged silica ions in the form of monomers and polymers. This results in formation of electrical double layers adjacent to the silanol groups, which further control dissociation, being sensitive the alkali/calcium ratio in the fluid. Gelation is facilitated by polymerisation of the silica ions through cross-linking by Ca^{2+} ions derived from portlandite [17,23,24], because Ca^{2+} has a higher affinity for the silica ions than the monovalent alkali ions [22,25].

The swelling pressures of ASR-gels depend on their Na, K, Ca, Si and water contents. Gels are very low permeable bi-continuous liquid-solid systems of colloidal dimensions: one can “move” from the solid to the liquid by moving just few nanometres. The bonding reactions in gels are virtually irreversible, being far from equilibrium with its surroundings: The elasticity modulus of Si-Ca-rich gels increases in proportion to the volume fraction of the solid i.e., the strength is negatively correlated with the water contents [26]. Calculations of the Na-Si-water system has shown that the viscosity of ASR-gels increases strongly with increasing SiO_2/H_2O-ratios at moderately low Na contents, and gels with high Na contents have low viscosities, irrespective of the SiO_2/H_2O-ratio [27]. This is consistent with Kawamura and Iwahori [28] who found that alkali-rich gels showed low swelling pressure and high free swelling, whilst gels with moderate to low alkali contents exerted a pressure under constraint. The gel swelling mechanism has been explained by osmosis [3,29], chemical potential gradients causing water imbibition [30] or electrical double layer repulsion [18]. As yet no consensus has been reached. Moreover, the additional effect of volumetric accumulation of gels on total ASR expansion appears to be a neglected research field.

Hagelia [2] found a negative linear correlation of SiO_2 and water in gels within RILEM AAR-2 samples (Accelerated Mortar-Bar Test Method for Aggregates) [31], suggesting that ASR gels are two component mixtures of Si-O-OH (bridged by Ca) and a liquid with alkalis attached to electrical double layers. Exuded non-viscous gels contained much more water than the internal gels that had caused expansion. It was proposed that development of gels with a high internal swelling pressure may only take place within a highly polymerized viscoelastic and negatively charged Si-rich network with an appreciable amount of

confined liquid with alkalis, leading to swelling by electric double layer repulsion [2]. This model is compatible with highly deprotonated silanol groups at high pH [22,32] and that most water resides in pores within the amorphous network [33]. Recent investigations of ASR-gels [3,34] demonstrated complex relations between gel rheological properties and composition, as based on the physical properties of 20 different synthetic ASR gels, with molar ratios of Ca/Si, Na/Si and K/Si ranging from 0.05-0.5, 0.1-1.0 and 0.0-0.3, respectively. Statistical handling showed that compressive strength, yield stress and viscosity increased with increasing Ca/Si molar ratios up to about 0.27-0.3, beyond which these parameters dropped again. Very low alkali/Si-ratios corresponded to high gel compressive strengths and yield stress. Increasing Na/Si and K/Si ratios leads to increased water absorption to ASR-gels and free swelling, which reduces the yield strength and swelling pressure. Equations were calibrated for estimation of gel swelling pressure and gel compressive strength. The model's accuracy for predicting swelling pressure and compressive strength from observations was estimated to be within 78 % and 74 % confidence, respectively [3]. The highest gel swelling pressures were found at very high alkali/Si-ratios yet depending much on the Ca/Si-ratios [34].

In the present paper petrographic details of ASR reaction products are combined with their relationship to microcracks and voids within cement pastes and aggregates from several settings, with emphasis on small-scale chemical variation. We calculated gel compressive strengths according to Eq. 6-12 in [3] and gel swelling pressures, using Eq. 2 in [34], and discuss the micro-scale evolution, gel accumulation and storage, crack formation and the potential mobility of ASR-gels.

2. MATERIALS AND METHODS

The study was based on thin sections selected from three Norwegian bridges and one concrete prism after performance of laboratory expansion tests of a Portuguese granitic aggregate. The Norwegian concretes were made with Portland cements corresponding to CEM likely with high $Na_2O_{eq} \approx 1.2$-1.3 wt. % and w/c-ratio about 0.5-0.6, which was commonly used at that time [7]. The Portuguese test sample, studied previously [35], was prepared and exposed according to standard procedures in the RILEM AAR-4.1 method [36] using CEMI 42.5 R from CIMPOR company with an alkali content ranging from 0.86 to 0.89% Na_2O_{eq}.

Concrete slices for the polished thin sections were prepared by using water as a coolant. Before impregnation the Norwegian specimen were dried at 60 ºC for 2 hours and the Portuguese were fast dried for 10 minutes at 70ºC. All the process is not automatic and is closely followed to guarantee the complete impregnation of the slices. The thin sections were first examined in polarised light under a conventional petrographic microscope. The focus was on gels and their micro-structural setting in the concrete aggregates and in the cement paste matrix. The thin sections were carbon coated using a VG MICROTECH E6700/T800. This was followed by SEM-EDS analysis under FEG-SEM: JEOL 7001F equipment and Oxford INCA 250 for EDS, using a 20 keV electron beam, and X-ray mapping for final selection of areas of interest.

Several points in each ASR reaction product were analysed by quantitative electron microprobe analysis (EPMA with WDS) performed at the University of Lisbon. Each area of interest was carefully checked by EDS Oxford INCA X-act, ensuring all relevant elements were analysed. The WDS operating conditions of the electron beam were current intensity of 1 nA, accelerating voltage of 15 keV, and 5 µm diameter of the electron beam, being little sensitive to sodium loss. Analytical points were from dense gels significantly apart from internal gel cracks and aggregate minerals. The instrument used, a JXA 8200 does not include a SXES superspectrometer (a high performance spectrometer for the light elements measurement). For minerals, in order to allow more accurate ZAF correction calculations, the unmeasured light elements are estimated from expected stoichiometry whenever possible (as for the case of B in tourmalines) and the reminder to 100% is postulated to be H_2O. In the case of glasses, gels, and not stoichiometrically defined materials in general, the unmeasured light elements cannot be estimated at all and the difference to 100% is always accounted as H_2O during ZAF corrections. Analysis totals of reaction products by EMPA were always less than 100 %, thus providing additional very important information on the possible liquid contents of individual gels. Sample preparation does potentially influence the water content, as well as the vacuum used for the conductive coating and the observation under SEM and EPMA. However, it has been established that gels are very low permeable bi-continuous liquid-solid systems, being far from equilibrium with their surroundings [26] and that most water resides in pores within the amorphous network [33]. Therefore, it was assumed that the difference from 100 % minus totals of other elements essentially represents structurally bound or confined water,

and potentially also non-bound water in capillary pores having been replaced by epoxy during preparation.

We calculated gel compressive strengths (σ_c) from molar ratios according to Equation 1 [3] and restrained swelling pressures (P_{rs}) according to Equation 2 [34]. Their calibration variation is restricted to ratios of Ca/Si, Na/Si and K/Si ranging from 0.05-0.5, 0.1-1.0 and 0.0-0.3, respectively.

$$\sqrt{\sigma_c} = 2.587 + 11.73\frac{Ca}{Si} - 1.661\frac{Na}{Si} - 6.96\frac{K}{Si} - 18.14\left(\frac{Ca}{Si}\right)^2 - 4.56\left(\frac{Ca}{Si}\right)\left(\frac{Na}{Si}\right) + 13.66\left(\frac{Ca}{Si}\right)\left(\frac{K}{Si}\right) \quad (1)$$

$$\ln\left(P_{rs}(MPa)\right) = 3.85 - 1.0\frac{Ca}{Si} - 45.5\frac{Na}{Si} - 2.1\frac{K}{Si} - 35.6\left(\frac{Ca}{Si}\right)^2 + 72.9\left(\frac{Na}{Si}\right)^2 + 43.23\left(\frac{Ca}{Si}\right)\left(\frac{Na}{Si}\right) - 61.8\left(\frac{Ca}{Si}\right)\left(\frac{K}{Si}\right) + 38.5\left(\frac{Na}{Si}\right)\left(\frac{K}{Si}\right) - 43.2\left(\frac{Na}{Si}\right)^3 \quad (2)$$

3. RESULTS

3.1 Microstructure and gel chemistry

Concrete from the Norwegian Strandengen bridge (thin section 1.1); the Breivegen bridge (thin section 3A-1) and Henja bridge (thin section HE 9) were investigated. The concrete ages at the time of core extraction were 25, 40 and 55 years, respectively. Each thin section was taken from about 8 cm below the outer surface. The concretes at Strandengen and Breivegen were extensively affected by ASR, whilst being less advanced at Henja. The reacted aggregates were mainly mylonite and silty meta-sandstone (Strandengen); meta-arkose, mylonite, schist and phyllite (Breivegen) and mylonite (Henja). In addition, one Portuguese concrete prism (thin section GR2-4c) manufactured with a Hercynian Portuguese granite containing strained quartz was selected, after laboratory expansion test. The expansion of the prism was of 0.07 % after 20 weeks, being higher than the threshold value of 0.03 % according to RILEM AAR-4.1 (60 °C Test Method for Aggregate Combinations Using Concrete Prisms) [36].

There was a very significant variation in gel chemical composition within each investigated domain. Crystalline reaction products locally occurred in close association with the amorphous gel. The gel composition to a great extent reflected the ambient environment, being dependent on variations in aggregate mineralogy, proximity to cement paste and proximity to open unfilled cracks and air voids.

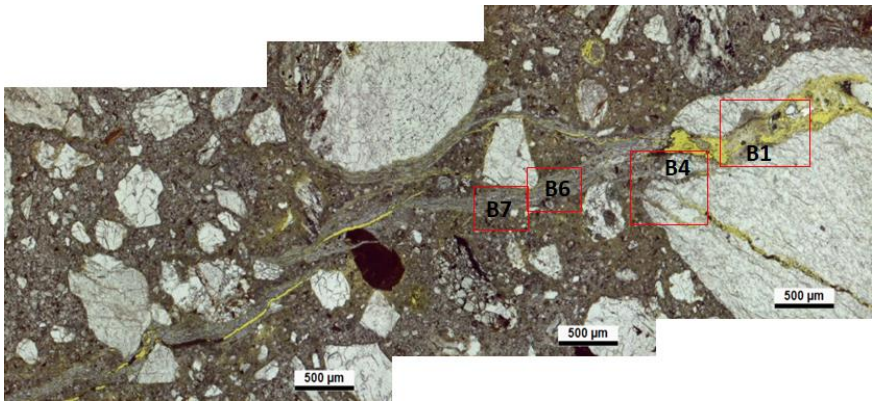

Figure 3.1: Parts of thin section 1.1 with areas of interest, observed in plane polarized light

Some main aspects of gel development in the Strandengen bridge are shown in Figure 3.1 which illustrates the encountered research topic. Grey layered (laminar) gels fill cracks in the cement paste completely, whilst gels within aggregate particles display variable degree of fill and with frequent occurrence of open cracks without gel inside the aggregates. In a similar fashion, air voids were only partly filled with ASR gels.

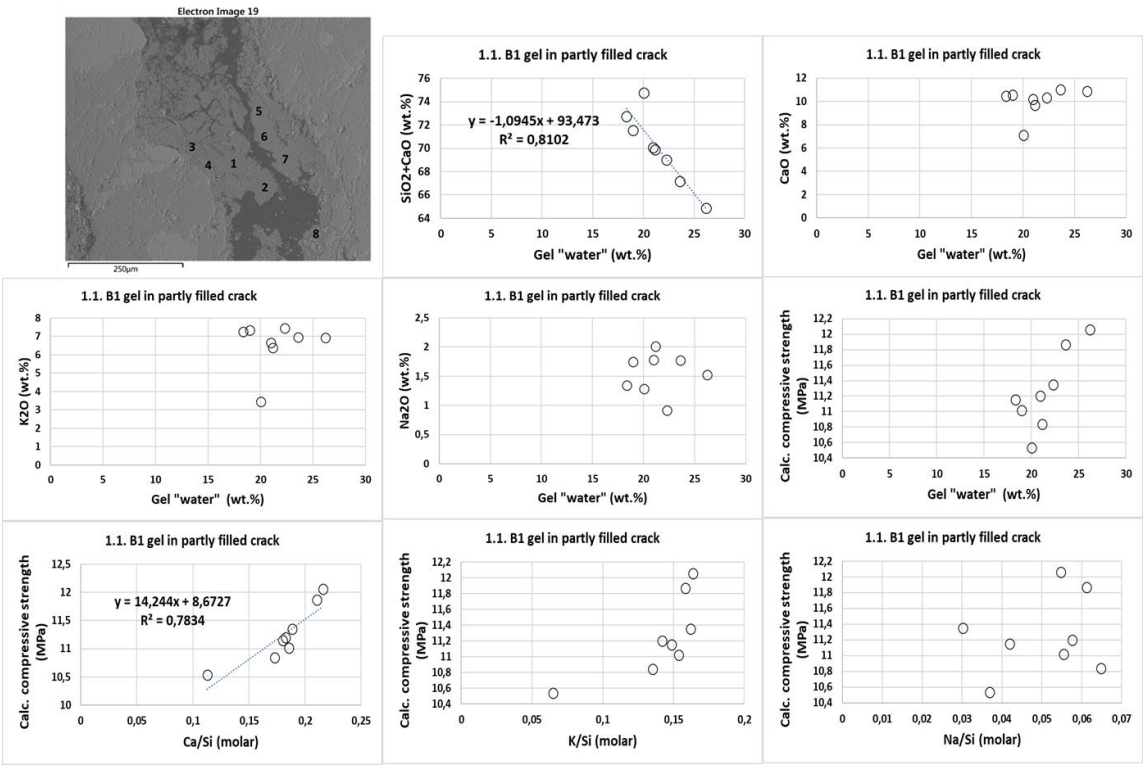

Figure 3.2: 1.1-B1. Gel partly filling a possibly pre-existing crack or flaw crossing the foliation of a mylonitic aggregate particle with quartz grain sizes 50-100 µm. Scale bar = 250 µm

Case 1.1-B1 (Figure 3.2): A big gel party filling a 250 µm wide crack within a mylonitic aggregate particle. This gel occurs along the same crack as the large laminar gel within the cement paste (B6/B7). Parts of gel B1 was possibly lost in preparation. EMPA analyses focused on gels with high degree of fill in contact with quartz on either side. There was a good negative correlation of SiO_2+CaO and "water". However, "water" was not correlated with CaO, K_2O and Na_2O. Calculated gel compressive strengths ranged from 10.5 to 12 MPa and increased with the Ca/Si-ratios, which is compatible with the results of [3] within this range. The highest strengths and the highest Ca/Si were related to points 3 and 4 nearest the aggregate, whilst the lowest strength was obtained from pt. 8 with the lowest Ca/Si and low "water" near the empty space of the crack. The gel strength increased with increasing K/Si-ratios and "water", whilst there was no such correlation with the Na/Si-ratio. Al_2O_3, which might reduce expansion of gels [18], was low (0.05 to 0.18 wt. %) and did not correlate with the strength estimates.

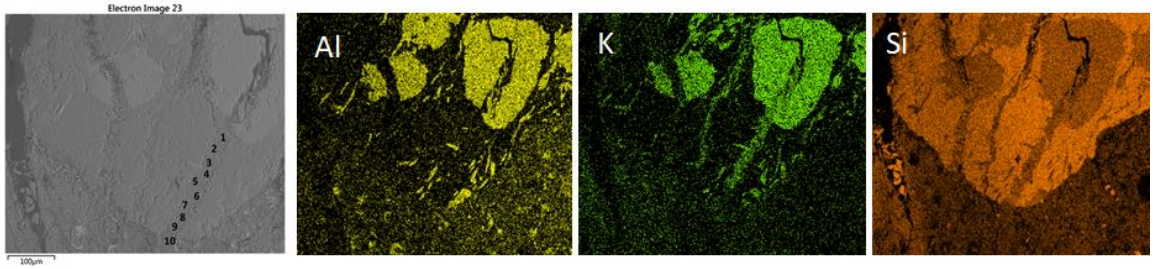

Figure 3.3: 1.1-B4. SEM-BSE image and X-ray maps of a single gel in a mylonitic aggregate with large K-feldspar porphyroclasts within a matrix of microcrystalline quartz and mica grains. Scale bar = 100 µm.

Case 1.1-B4 (Figure 3.3): Thin gel filling a 27 µm wide crack within mylonite aggregate and extending into the cement paste. Analytical points 1 & 2 in the innermost part were rich in K_2O (ca 7.5 wt. %) and contained a little Al_2O_3 (ca. 0.2 wt. %), reflecting dissolution of adjacent potassic feldspar. In contrast, points 8, 9 & 10 close to the cement paste within quartz had the lowest CaO (ca. 7.3 %), K_2O (ca 1-2

%), Na_2O (ca. 1.2 %) and Al_2O_3 (ca. 0.1. %), with very *high* Si (SiO_2 ca. 71 %), reflecting local contribution of quartz. The intermediate analytical points 3 to 7 with higher CaO (ca 12 %), K_2O (6.4 to 7.5 %), Na_2O (ca. 0.5 %) and Al_2O_3 (ca. 0.3 to 1 wt. %), showed possible influence of local mica. The latter gels showed a negative correlation between SiO_2+CaO and "water", falling close to Case 1.1-B1. The overall gel showed a very scattered positive correlation of Ca, K, and Na with gel "water". Calculated gel compressive strengths ranged from about 12 to 14 MPa and increased with the Ca/Si-ratios, with a very scattered positive correlation with the "water" contents. There was no clear correlation between calculated strengths and the alkali/Si-ratios and Al contents. The highest strengths and the highest Ca/Si (= 0.26) were indicated in points 2 and 6, whilst the *lowest strength* and the lowest Ca/Si (due to high Si derived from quartz) was obtained in points 8 to 10 *near the cement paste*.

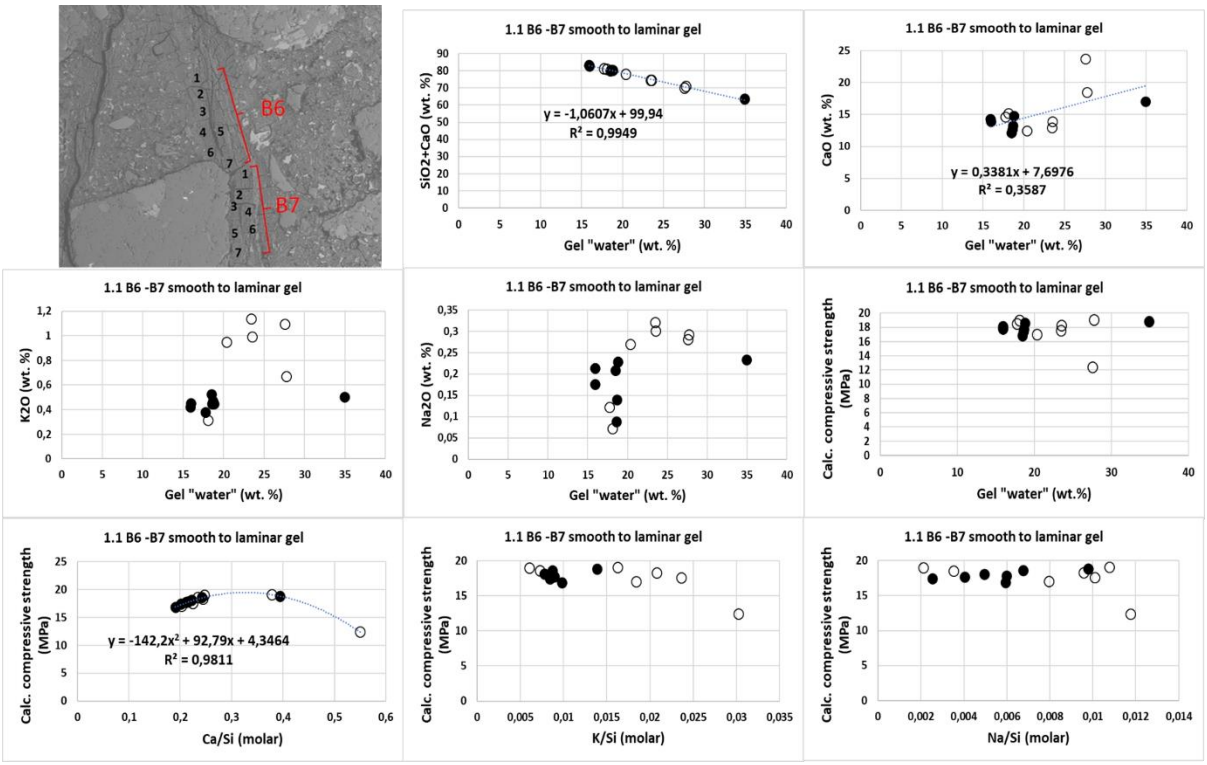

Figure 3.4: 1.1-B6-B7. Thick laminar gel within the cement paste and in contact with quartz-rich aggregate. Width of BSE image = 1600 µm. Analysed points in B6 (open symbols) and B7 (filled symbols).

<u>*Case 1.1-B6-B7 (Figure 3.4): A ca 220-230 µm thick layered gel crossing through the cement paste as an extension of the crack in 1.1. B1.*</u> B6 represents a part of the gel with cement paste on either side, whilst area B7 of this gel is in contact with a quartz-rich aggregate on one side. The overall chemical variation shows that this thick gel with layers parallel to the crack, reflects the local micro-environment. Except for points 6 and 7 in B6, being close to the aggregate, K_2O, Na_2O, CaO and "water" was higher than in B7, hence reflecting higher impact of the cement paste in B6 than in B7. The analyses of 1.1-B6 showed that SiO_2 dropped gently from 65.6 to 46.2 wt. % (points 1 through 5). However, point 6 and 7 located closest to quartz had higher SiO_2 (66.6 and 65.9 %), being similar to the SiO_2 contents in B7 (ca. 65 %), reflecting stronger impact of quartz dissolution. There was a good negative linear correlation of SiO_2+CaO and "water" (R^2 = 0.99). The gel "water" is poorly correlated with CaO, whilst K_2O and Na_2O versus "water" show curve-shaped relationships with positive correlation from 15 % to about 25 % "water". The calculated gel compressive strengths varied between 16.9 and 19 MPa, with the exception of point 5 in B6 with Al_2O_3 = 0.59 % which yielded 12.4 MPa. Otherwise, Al_2O_3 varied from 0.02 to 0.17 wt.%. Apparently, there was a negative linear correlation of Al_2O_3 and gel strength (R^2 = 0.75, not shown). The calculated gel strengths formed a curve with the highest strength at Ca/Si about 0.3. This ratio did not correlate with the "water" contents. The strengths were independent on the Na/Si and K/Si-ratios, except for at the highest alkali/Si-ratios.

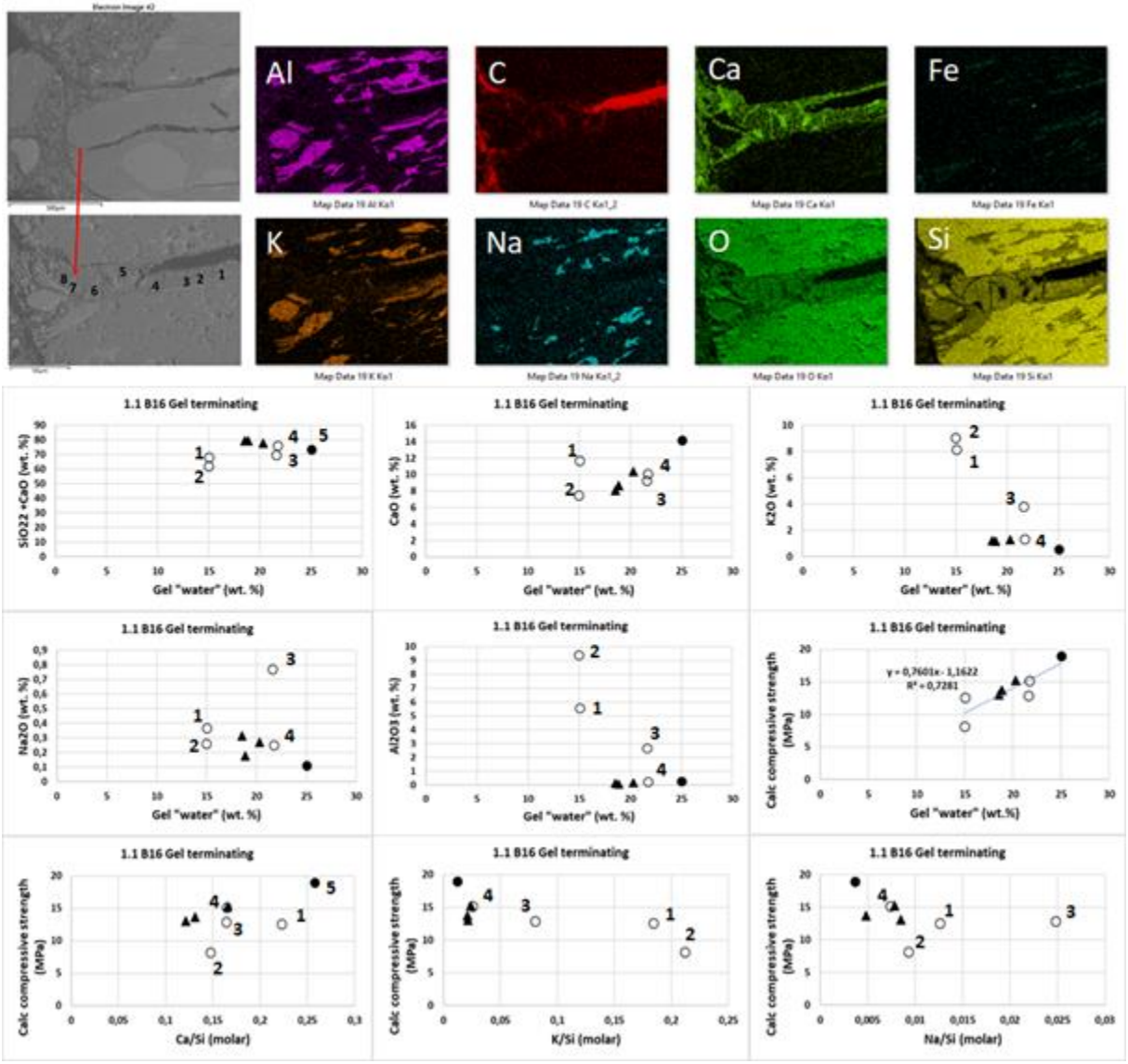

Figure 3.5: 1.1-B16. SEM-BSE image and X-ray maps of a single gel partly filling a crack in an aggregate particle of mylonitic gneiss. The gel was terminating at the interface with the cement paste. Notice the presence of K-feldspar (Al = pink, K = orange) and quartz. Open circles = gel close to the open crack; Filled triangles = gel near the cement paste; Filled circles = gel in intermediate positions. Scale bar of lower back scatter image = 50 µm.

Case 1.1-B16 (Figure 3.5): A 20-25 µm wide gel terminating both at the aggregate/cement paste interface and towards an empty crack inside a mylonitic aggregate. The gel termination towards the inner open crack was embayed, suggesting limitation to growth and the termination against the cement paste matrix was sharp. There was no general negative correlation of SiO_2+CaO and "water", whilst analyses of gel points towards the cement paste fell close to the trend in Figure 3.4 (e.g., points 4 to 8): All these points had low Al contents (Al_2O_3 = 0.06 to 0.24 %). In contrast, the Al_2O_3 contents at the inner gel terminations were very high (5.54, 9.36 and 2.64 in points 1, 2 and 3, respectively), with a negative linear correlation of Al_2O_3 and compressive strength (R^2 = 0.64). Points 1 and 2 at the innermost parts near the open crack had the lowest "water" contents, the highest Al and K, reflecting influence of K-feldspar and some muscovite in the immediate vicinity. Ca mainly increased with gel "water", whilst K/Si and Na/Si-ratios were mainly negatively correlated with "water". Calculated compressive strengths in outer gel increased from 13.0 to 18.9 MPa with Ca/Si-ratios ranging from 0.13 to 0.26, whilst gel strengths in Al-rich points near the termination inside the aggregate ranged from 8.1 to 12.9 MPa. All single point analyses showed a significant positive linear correlation between gel compressive strength and "water" contents (R^2 = 0.73).

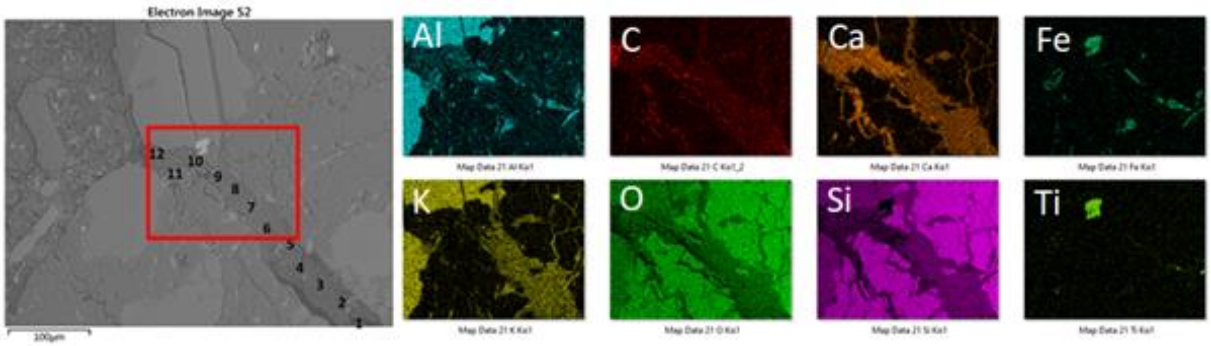

Figure 3.6: 3A-1-B1. SEM-BSE image and X-ray maps of a single gel filling a crack within an aggregate mainly consisting of quartz (Si = pink) and K-feldspar (Al = blue, K = yellow) showing full termination at the interface with cement paste with locally elevated Ca contents (orange). Scale bar (BSE image) = 100 µm.

Case 3A-1-B1 (Figure 3.6): A ca 20-25 µm gel within a crack terminating at the aggregate/cement paste interface. The outer and inner parts of the gels were located within K-feldspar, whilst the middle part was located in quartz. The analytical points 11 and 12 closest to the cement paste showed very elevated Al_2O_3 (4.4–5.5 %) and CaO (21-25 %) with somewhat low K_2O (1.3-1.6 %), suggesting influence from cement and feldspars. Also, inner points 1, 2 and 3 near K-feldspar had somewhat elevated Al_2O_3 (0.6 – 1.30 %) with somewhat low K_2O (2.8-2.9 %) and CaO (9.6-11.1 %) compared to the remaining domains in presence of quartz (Al_2O_3 = 0.25-0.70 %, K_2O = 3.9 – 6.5 % and CaO = 11.1-13.6 %). Ca, K and Na were negatively correlated with the "water" contents. There was a good negative linear correlation of SiO_2+CaO and "water" (R^2 = 0.96), coinciding well the trends in 1.1. B1 and 1.1. B6/B7. Calculated gel compressive strengths for most microdomains clustered around 15 MPa at Ca/Si = 0.24. In contrast the apparent strength in the outermost gels (11 & 12) were 8.4 and 0.5 MPa, respectively, with Ca/Si-ratios 0.6 to 0.78, however, the latter clearly outside the calibration range of the equations. There was an overall scattered negative correlation of gel strength and Al-contents.

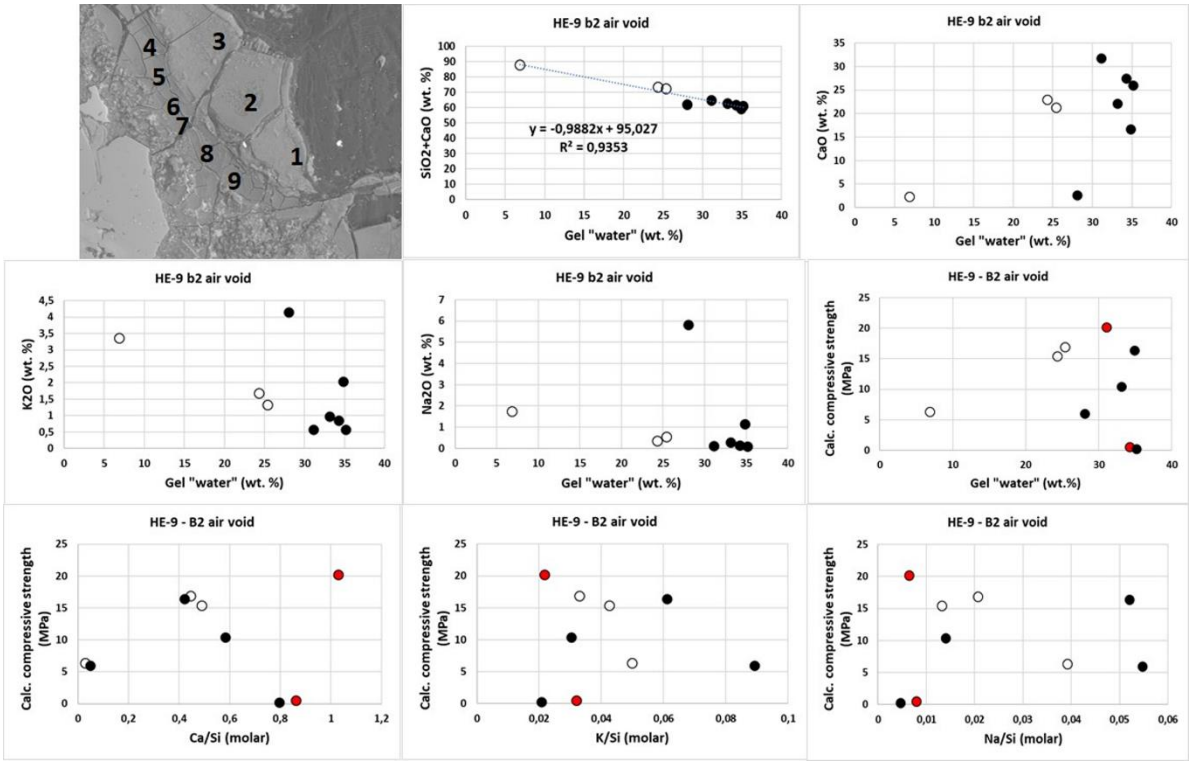

Figure 3.7: Image shows part of an air void, with early gel along the margin with cement paste (filled circles) and later gel towards open space (open circles = points 1,2 & 3). Red symbols = square root of compressive strengths were negative, well outside the calibration range. Image width = 500 µm.

Case HE-9 B2 (Figure 3.7): Layered gels partly filling an air void. The gels were dense and consisted of two successive layers. The early formed gel in contact with the cement paste had a very variable Ca, K and Na contents, with larger variation than in the late-stage gel (points 1 to 3). There was a very good negative linear correlation between SiO_2+CaO and "water" (R^2 = 0.94). Each layer apparently define correlations of Ca, K and Na with "water". Calculated gel compressive strengths did not correlate with the "water" contents and the Ca/Si, K/Si and Na/Si-ratios. Two analysed points of early gel were far outside the calibration range of the equations (red symbols). However, both early and late-stage gels with Ca/Si-ratios between 0.05 and 0.58 form a trend quite close to those in 1.1 B6/B7 with strength varying from 6 to 16 MPa. Al_2O_3 was high in the early formed gel (2.36-3.73 %) and low in the late-stage gel (0.02-0.06%). There was no correlation between calculated strengths and Al-contents (not shown).

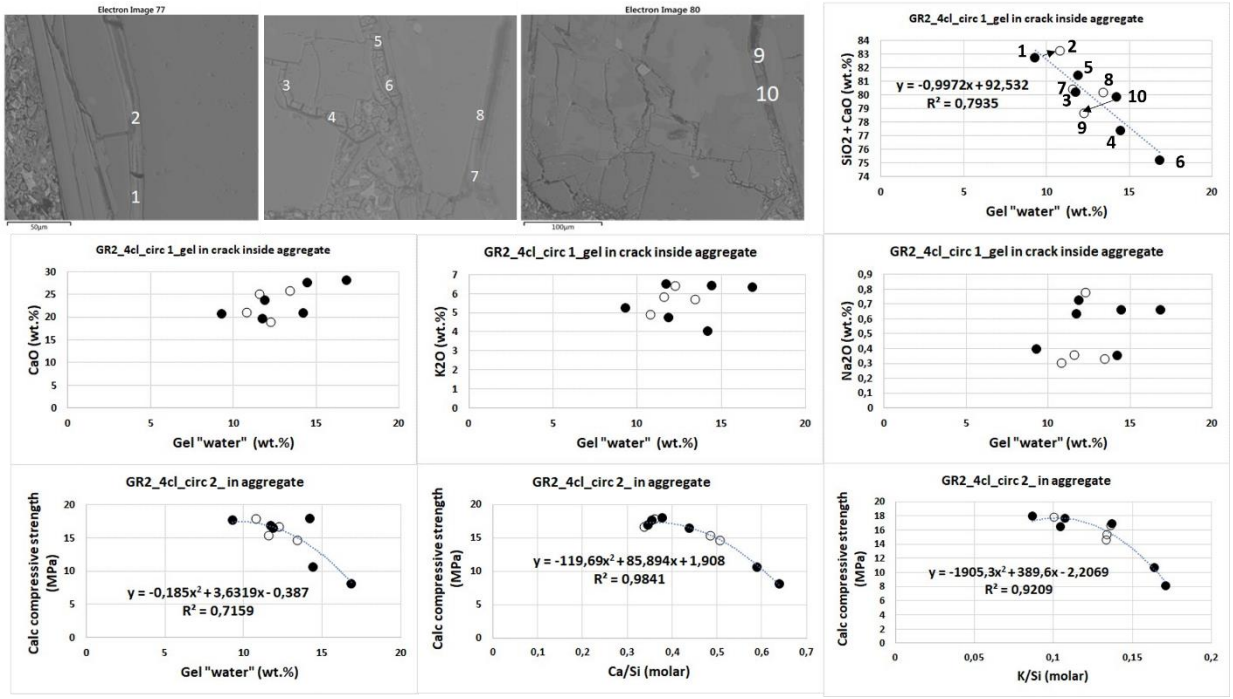

Figure 3.8: Arrows show tie lines between compositions of gels that filled cracks completely (filled circles) and compositions near the open cracks. Image widths = 200, and 400 µm, respectively.

Case GR2-4cl-1 (Figure 3.8): Gels within aggregate cracks. Several gels had formed within granitic aggregates, including domains of feldspars. Some gels terminated inward towards partly filled cracks. There was a fairly good negative correlation of SiO_2+CaO versus "water" (R^2 = 0.79) , but apparently without a systematic change in composition between the gels that filled the cracks completely and the ones near their termination against partly filled crack (see tie lines in Figure 3.8). Despite being located within feldspars the Al_2O_3 was at 0 %, with the exception of sample point 1 (Al_2O_3 = 0.18 %) %). The calculated gel compressive strengths were forming a curve with the highest strength at a Ca/Si-ratio about 0.35, clearly resembling features in 1.1 B6/B7 and other structural concretes. The strength versus "water", Ca/Si, K/Si and Na/Si (not shown) also describe curves with polynomial fits.

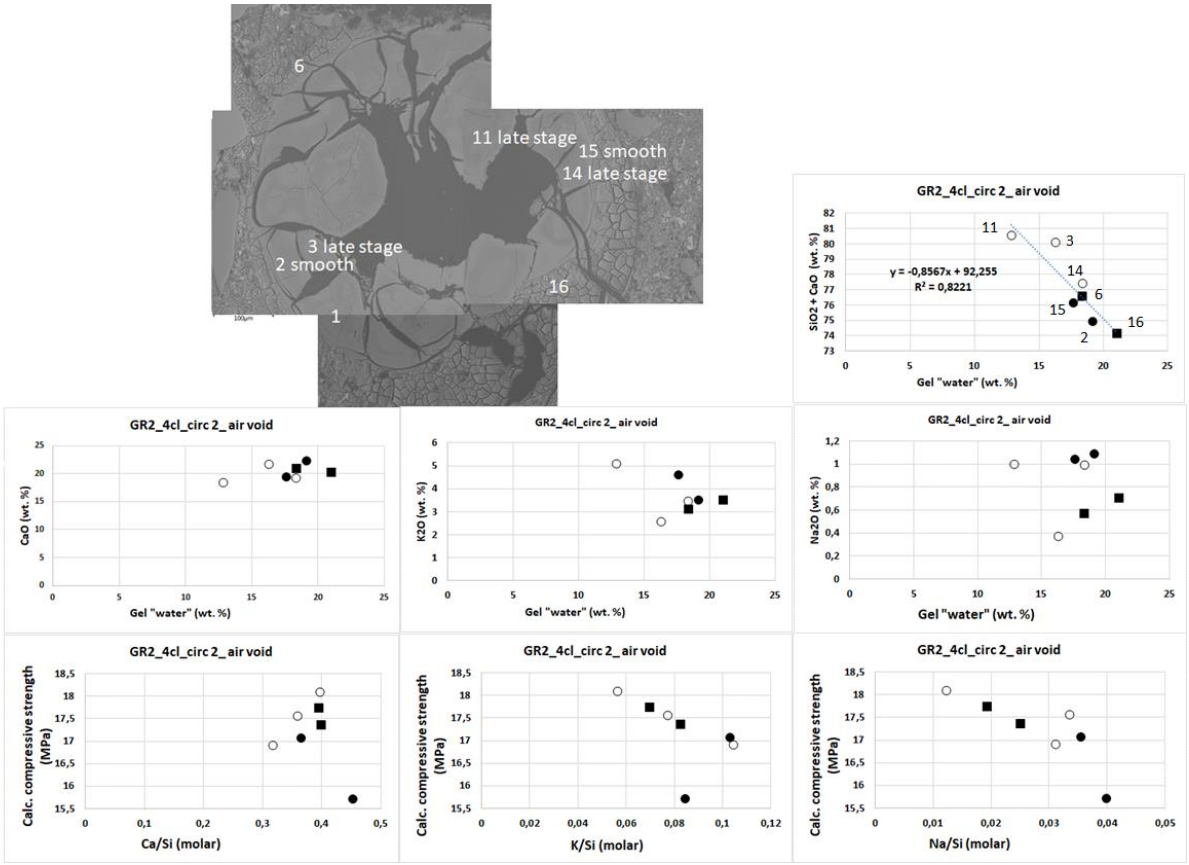

Figure 3.9: Early formed gel (filled squares); smooth gels (filled circles) and late-stage gels within smooth gels (open and grey circles). Scale bar = 100 µm.

Case GR2-4cl-2 (Figure 3.9): A large gel partly filling an air void. Three types of gel were observed; Early formed cracked gel and later formed smooth/dense gel with internal late-stage gel. All gels contained similar high Ca. The early formed gel in contact with the cement paste had quite uniform K and Na contents, whilst later stage gels had variably higher alkali contents. There was a good negative linear correlation between SiO_2+CaO and "water" (R^2 = 0.82), and the late-stage gels had less "water". Calculated gel compressive strengths in early-stage; smooth and late-stage gels were 17.3-17.7 MPa; 15.7-17.1 MPa and 16.9-18.1 MPa, respectively. With exception of one smooth gel, the strengths were positively correlated with the Ca/Si-ratios from 0.3-0.4 and negatively correlated with the alkali/Si-ratios. There was no correlation between strength and "water" and Al_2O_3 (0.17-0.36 %).

3.2 Gel strengths and pressures in different micro domains

Table 3.1 gives a summary of the microstructural setting of the ASR-gels and average apparent gel compressive strengths and swelling pressures for characteristic microdomains. However, the significant compositional variation in each case may well imply variable gel compressive strengths and gel swelling pressures, even within single gels. The gel strengths mainly fall between 10 and 20 MPa, reflecting high viscoelasticity. The layered gels in 1.1 B6/B7 within the cement paste have the highest strength. Similar strengths were also reached in the central parts of the gel 1.1 B16 and composite gels in air void GR2-4c-2. Yet, the swelling pressures are surprisingly low, ranging from 0.0 to 1 MPa. Despite this, most gels in these concretes had clearly caused deleterious expansion. The parts of crack-bound gels within aggregates which terminated at the cement paste tended to be a little weaker than the same gels farther inside. The very low compressive strength and swelling pressure in 3A-1 B1 (4.5 MPa/0.1 MPa) is possibly erroneously low, because the Ca/Si was well beyond the calibration range. However, there were also indications that significant incorporation of Al has caused a reduced strength.

Table 3.1: Main results based on several individual analyses of each gel in different microstructural settings. Each thin section area represents a continuous gel. n = number of analytical points.

Thin section area	Microstructural setting of gels	Layer thick-ness of gel (µm)	State of fill in cracks or air voids (n)	Gel comp. strength (MPa)	Gel swelling pressure (MPa)
1.1 B1	Crack in aggregate crossing foliation and extending 3500 µm into the paste	250	Filled across crack but large empty crack (8)	11 ±3	0.4 ±0.3
1.1 B4	Crack in aggregate reaching 350 µm into the cement paste	27	Filled near paste (3) Filled in aggregate (7)	12 ± 3 13 ± 3	1± 0.2 0.2 ± 0.04
1.1 B6	In cement paste along same crack as B1	230	Filled in paste (7)	17 ± 4	0.8 ± 0.2
1.1 B7	In cement paste along same crack as B1	220	Filled in paste near aggregate (7)	17 ± 4	0.9 ± 0.2
1.1 B16	In aggregate between inner open crack and cement paste. Terminated at aggregate/paste interface	25	Filled near paste (3) Filled middle (2) Partly filled near open crack (3)	14 ±3 17 ± 4 11 ± 3	0.9 ± 0.2 0,8 ± 0.2 0.2 ± 0.04
3A-1 B1	In aggregate between inner open crack and cement paste. Terminated at aggregate/paste interface	45	Filled near paste (1) Filled, middle (6) Partly filled near open crack (4)	8 ± 2 14 ±3 15 ±3	0.1 ± 0.1 0.2 ± 0.04 0.4 ± 0.1
HE-9 B2	In air void	210	Partly filled: 1st deposit (6) 2nd deposit (3)	 9 ± 2 12 ±.3	 0.3 ± 0.1 0.6 ± 0.1
GR2-4c-1	Several thin gels in feldspar-rich aggregate	15	Filled to empty (10)	15 ± 3	0.0 ± 0.02
GR2-4c-2	In air void	200	Partly filled: 1st deposit (2) 2nd deposit (2) 3rd deposit (within 2nd) (3)	 17 ±.4 16 ±4 17 ± 4	 0.2 ± 0.04 0.2 ± 0.04 0.3 ± 0.1

Inspection of the diagrams (Ch. 3.1) shows that the parts of gels closest to open gel-free cracks in aggregates tended to have lower contents of “water” and calcium than the same gels filling the cracks. Also, the late-stage gels in air voids shared this feature. This suggests that gels near open spaces in cracks and voids gradually became isolated and depleted in Ca and “water”, which might be reflecting development towards inhibition of gel polymerisation through exhaustion of Ca. Yet, the gel next to the open cracks and voids had rather high compressive strengths. The gel near the open crack in 1.1. B16 obtained a little lower compressive strength (14 Ma) than the internal gel filling the same crack and the free swelling was only 0.2 MPa. In contrast, 3A-1 B1 has the highest compressive strength and the highest free swelling in the gel close to the open crack, being similar to the situation in air void HE-9 B2. The strength in the different air void gels in GR2-c2 were generally high, with low swelling pressures. In comparison the crack bound gels in GR2-c21 had a little lower strength and almost no swelling pressure.

4. DISCUSSION AND CONCLUSIONS

4.1 In situ formation of two-component ASR gels

The results obtained for the “water” content might be influenced by a number of processes as already referred, from the collection of the samples, the thin section preparation with “water” to sequent need

for drying. Also, the vacuum conditions as well as the current intensity used on these types of products containing and uncertain content of “water” may have an influence on the measurements. However, the vacuum conditions are similar to all the thin section analysed, affecting in a similar way the amorphous materials. For each thin section, the influence of the preparation is the same for all the areas analysed. In addition, there might have been some changes from the moment of formation of the gel and the performance of the analyses. The values of Na should be less affected as the EPMA is calibrated for stoichiometric minerals. The very good negative linear correlations between SiO_2+CaO and “water”, with regression coefficients (R^2) for individual gels ranging from (0.73) 0.81 to 0.99, suggest that gel “water” was not significantly influenced by preparation and that ASR gels are two-component mixtures of “water” and an amorphous network mainly consisting of Si and Ca.

The chemical composition of single ASR-gels depended strongly on the local micro-environment, reflecting the local aggregate mineralogy and the proximity to the cement paste both in crack bound gels within aggregates and in the cement paste. This suggests that these gels formed and acted more or less *in situ*. Furthermore, no textural evidence suggests movement of gels: the layering of the extensive gel in cement paste (1.1. B6/B7) represents sequential growth of gel layers within the crack, and that formation of successive layers had caused widening of this crack. In the hypothetical case of expulsion from the aggregate one would expect a much more complex gel microstructure.

4.2 A model for ASR-expansion by strong gels with low swelling pressures

A high swelling pressure (>2 MPa) exceeding the tensile strength of concrete is by most researchers regarded as a prerequisite for deleterious ASR. In the present case the estimated swelling pressures are mainly too low for splitting concrete, unless chemical strain softening can reduce the strength to less than half of the pristine strength. Assuming that the equations [3,34] are approximately correct and generally applicable, this calls upon another look at the expansion mechanism in ASR.

In general, internal expansion and cracking of concrete might result from 1) *either* precipitation of minerals with high molar volume, such as gypsum or ettringite, *or* 2) formation of a gel which exerts a sufficiently high pressure. *It is worth noting that pressure exerted by an ASR-gel is the sum of the swelling pressure and a separate effect from sequential accumulation of ASR-gel.* The latter seems little investigated. The effect of gel accumulation can be compared with crystallisation within a confined space. The molar volume of ASR-gels is apparently depending on their chemistry, and a K-C-S-H gel; of 77.5 cm^3/mole [37] seems relevant to our system. This is close to the molar volume of gypsum (74.56 cm^3/mole). Although gypsum compressive strength is approximately 10 times higher than the ASR-gels in this study (160 MPa), gel compressive strength in the order of 10-20 MPa seems to be typical [3] and must hence be strong enough to sustain expansion by gel accumulation by analogy with gypsum growth. ASR due to accumulation of such strong gels with very low swelling pressures can therefore likely develop according to the following scheme, which is in keeping with our results:

At first susceptible aggregate particles are attacked by the alkaline pore fluid in the cement paste, which carries Ca and alkalis. The first ASR-gels form at the aggregate/paste interface, and preferably develop along structural weaknesses such as weak foliation planes and pre-existing micro-cracks, where dissolution of silicates will take place, thereby enhancing the micro-cracks. Strong viscoelastic gels then form within the concrete aggregates leading to widening of the cracks upon sequential accumulation, even when their swelling pressures are very low. Sequential accumulation of gels on aggregate cracks represents a force in analogy with gypsum crystallization, leading to accentuation of the cracks and a sustained attack. After their first formation at the cement paste/aggregate interface, gels accumulate inwards while filling and accentuating the cracks and also quite frequently terminated towards the inner parts of remaining open cracks when being gradually exhausted in Ca and “water”. A similar mechanism had been observed where thaumasite plugs have precipitated along the margin of aggregates and caused formation of open internal cracks without precipitates [38]. When gel accumulation within the aggregates is very high, the already formed aggregate cracks will propagate further into the cement paste. Subsequentially, gel will form layers on new formed cracks in the cement paste. Upon growth, this results in a layered (laminated) strong gel with swelling pressure < 1 MPa, which expands the cracks in the cement paste by further sequential accumulation. By contrast, if gel accumulation and strength is moderate, cracks initially formed within the aggregates may probably not propagate into the paste but terminate at the aggregate/cement paste interface.

It might be concluded that ASR-research should focus more on the microtextural evidence and microscale chemical variations within single gels. The present study has demonstrated that there is a huge potential for further work along these lines.

Acknowledgements

The authors thank Per Geir Sigursen (NPRA) and Mufak Said Naoroz (University of Oslo) for preparing thin sections. Also António Santos Silva, from National Laboratory for Civil Engineering, is acknowledged for providing the Portuguese sample produced in the scope of the IMPROVE project (Improvement of performance of aggregates in the inhibition of alkali-aggregate reactions in concrete - PTDC/ECM/115486/2009). Technical assistance by Pedro Rodrigues and Isabel Nogueira with EPMA analyses and SEM is gratefully acknowledged. This work was funded by FCT through the project UIDB/50019/2020 – IDL.

5. REFERENCES

[1] Poole AB, Sims I (2015) Concrete Petrography. A handbook of investigative techniques, 2nd ed. CRC Press, Taylor & Francis Group.

[2] Hagelia P (2008) Chemistry of ASR-gels and pore fluids in ultra-accelerated mortar bars: Evidence for Si-control on gel expansion properties. In: Broekmans MATM, Wigum BJ (eds.). Proc. 13th ICAAR, Trondheim, Norway, pp 697-707.

[3] Gholizadeh-Vayghan A (2017) Characterisation of the rheological and swelling properties of synthetic alkali silicate gels in order to predict their behaviour in ASR damaged concrete. PhD-thesis, The Pennsylvania State University, 226 pp.

[4] Visvesvaraya HC, Mullick AH, Samuel G, Sinha SK, Wason RC (1986) Alkali reactivity of granitic rock aggregates. Proc. 8th Congr. Chem. Cements, Vol. 208.

[5] Constantiner D, Diamond S (2003) Alkali release from feldspars into pore solutions. Cem Conc Res 33:549-554.

[6] Bérubé M-A, Fournier B (2004) Alkali releasable by aggregate in concrete – Significance and test methods. In: Tang M, Deng M (editors) Proc. 12th ICAAR, Beijing, China, Vol 1:17-30.

[7] Jensen V (1993) Alkali Aggregate Reaction in Southern Norway. Dr. Techicae thesis, Norwegian Institute of Technology, University of Trondheim.

[8] Fernandes I (2009) Composition of alkali-silica reaction products at different locations within concrete structures. Mat Charact 60:655-668.

[9] Werner D, Gardei A, Simon S, Meng B (2015) Microscopic investigation of building materials affected by alkali-silica reaction. In: O. Çoporoğlu (ed.). Proc. 15th Euroseminar on Microscopy Applied to Building Materials, Delft, The Netherlands, pp 183-190.

[10] Knudsen T, Thaulow, N (1975) Quantitative microanalyses of alkali-silica gel in concrete. Cem Conc Res 5:443-454.

[11] Shakoorioskooie M, Griffa M, Leemann A, Zboray R, Lura P (2021) Alkali-silica reaction products and cracks: X-ray micro-tomography-based analysis of their spatial-temporal evolution at a mesoscale. Cem Conc Res 150, 106593.

[12] Hagelia P, Fernandes I (2012) On the AAR susceptibility of granitic and quartzitic aggregates in view of petrographic characteristics and accelerated testing. In: Drimalas T, Ideker J, Fournier B (eds.). Proc. 14th ICAAR, Austin, Texas, USA, 10 pp.

[13] El Bitouri Y, F. Jamin F, Pe´lissou C, El Youssouf MS (2017) Tensile and shear bond strength between cement paste and aggregate subjected to high temperature. Materials and Structures 50:234.

[14] Jebli M, Jamin F, Malachanne E, Garcia-Diaz E, El Youssouf MS (2018) Experimental characterization of mechanical properties of the cement-aggregate interface in concrete. Const Build Mat, Elsevier, 2018, 161, pp.16 -25.ff10.1016/j.conbuildmat.2017.11.100ff. ffhal-01772491f.

[15] Ishii E (2015) Predictions of the highest potential transmissivity of fractures in fault zones from rock rheology: Preliminary results. J Geophys Res Solid Earth, 120, doi:10.1002/2014JB011756.

[16] Diamond S, Barneyback RS, Struble LJ (1981) On the physics and chemistry of alkali-silica reactions. In: Oberholster RE (ed.). Proc. 5th ICAAR, Cape Town, South Africa, 11 pp.

[17] Diamond S (1989) ASR-Another look at mechanisms. In: Okada K, Nishibayashi S, Kawamura M (eds.). Proc. 8th ICAAR, Kyoto, Japan, pp 83-94.

[18] Prezzi M, Monteiro PJM, Sposito G (1997) The Alkali-silica reaction, Part I: Use of the double-layer theory to explain the behavior of reaction products gels. ACI Mat J/January-February, pp 10-16.

[19] Griggs D (1967) Hydrolytic weakening of quartz and other silicates. Geophys J R Astr Soc, 14:19-31.

[20] Bulteel D, Riche J, Garcia-Diaz E, Rafai N, Degrugilliers P (2004) Better understanding of ASR mechanisms thanks to petrography study on altered flint aggregate. In: Tang M, Deng M (eds.): Proc. 12th ICAAR, Beijing, China, Vol. I, pp 69-78.

[21] Fournier B, Berube M-A, Folliard K, Thomas MDA (2010) Report on the Diagnosis, Prognosis, and Mitigation of Alkali-Silica Reaction (ASR) in Transportation Structures, Federal Highway Administration, Washington, DC.

[22] Dove PM, Rimstidt JD (1994) Silica – water interactions. In: Heaney PJ, Prewitt CT, Gibbs GW (eds.). Silica. Rev Min, Mineralogical Society of America 29:259-308.

[23] Thomas MDA (1998) The role of calcium in alkali silica reaction. Materials Science of Concrete: Special Volume – The Sidney Diamond Symposium. Cohen MD, Mindess S, Skalny JP (eds.), Am Cer Soc:325-337.

[24] Gaboriaud F, Nonat A, Chaumont D, Craievich A (1999) Aggregation and gel formation in basic silico-calco-alkaline solutions studied. A SAXS, SANS and ELS study. J Phys Chem 102:5775-5581.

[25] Wang H, Gillott HE (1991) Mechanism of alkali-silica reaction and the significance of calcium hydroxide. Cem Conc Res, 21:647-654.

[26] Scheerer G (1999) Structure and properties of gels. Cem Conc Res 29:1149-1157.

[27] Moore AE (1978) An attempt to predict the maximum forces that could be generated by alkali-silica reactions. In: Diamond S (editor) Proc. 4th ICAAR, Purdue University, USA, pp 363-368.

[28] Kawamura M, Iwahori K (2004) ASR gel composition and expansive pressure of mortars under restraint. Cem Conc Comp 26:47-56.

[29] Powers TC, Steinour HH (1955) An interpretation of some published researches on alkali-aggregate reaction 2 – An hypothesis concerning safe and unsafe reactions with reactive silica in concrete. J ACI Proc 51:785-811.

[30] Dent Glasser LS, Kataoka N (1981) The chemistry of alkali-aggregate reactions. Proc. 5th ICAAR, Cape Town, South Africa, S252/23.

[31] RILEM Recommended Test Method: AAR-2—Detection of Potential Alkali-Reactivity—Accelerated Mortar-Bar Test Method for Aggregates. In: Nixon P. Sim I. RILEM Recommendations for the Prevention of Damage by Alkali-Aggregate Reactions in New Concrete Structures (pp.61-77).

[32] Krattiger N, Lothenbach B, Churakov SV (2021) Sorption and electrical properties of ASR product and C-S-H: A comparative modelling study. Cem Conc Res 146:106491.

[33] Benmore CJ, Monteiro PJM (2010) The structure of Alkali silicate gel by total scattering methods. Cem Conc Res 40:892-897.

[34] Gholizadeh-Vayghan A, Rajabipour F (2017) Quantifying the swelling properties of alkali-silica reaction (ASR) gels as a function of their composition. J ACI 100:3801–3818.

[35] Ramos V, Fernandes I, Noronha F, Santos Silva A, Soares D, Leal S, Fournier B (2016) Assessment of the potential reactivity of granitic rocks. Petrography and expansion tests. Cem Concr Res 86:63–77.

[36] RILEM Recommended Test Method: AAR-4.1—Detection of Potential Alkali-Reactivity—60 °C Test Method for Aggregate Combinations Using Concrete Prisms. In: Nixon P. Sim I. RILEM Recommendations for the Prevention of Damage by Alkali-Aggregate Reactions in New Concrete Structures (pp.99-116).

[37] Shi Z, Ma B, Lothenbach, B (2021) Effect of Al on the formation and structure of alkali-silica reaction products. Cem Conc Res 140:106311.

[38] Hagelia P, Sibbick RG (2009) Thaumasite Sulfate Attack, Popcorn Calcite Deposition and Acid Attack in concrete stored at the “Blindtarmen” test site Oslo, from 1952 to 1982. Mat Charact 25:839-846.